Electronic Supplementary Information

Using an environmentally-relevant panel of Gram-negative bacteria to assess the toxicity of polyallylamine hydrochloride-wrapped gold nanoparticles

Joseph T. Buchman,[a] Ali Rahnamoun,[b] Kaitlin M. Landy,[a] Xi Zhang,[c] Ariane M. Vartanian,[c] Lisa M. Jacob,[c] Catherine J. Murphy,[c] Rigoberto Hernandez,[b] and Christy L. Haynes[a]

[a]Department of Chemistry, University of Minnesota, Minneapolis, MN 55455, USA

[b]Department of Chemistry, Johns Hopkins University, Baltimore, MD 21218, USA

[c]Department of Chemistry, University of Illinois at Urbana-Champaign, Urbana, IL 61801, USA

S1. Known Lipopolysaccharide Structures from the Bacterial Panel

While the structures of the LPS of all the bacteria in the panel are not fully characterized, those from *P. aeruginosa* PAO1, *S. oneidensis* MR-1, and *S. oneidensis* MR-4 have been characterized. These structures are shown in Fig. S1 and can be used to calculate the charge of each bacteria's LPS. TEM images of each bacterium are also shown.

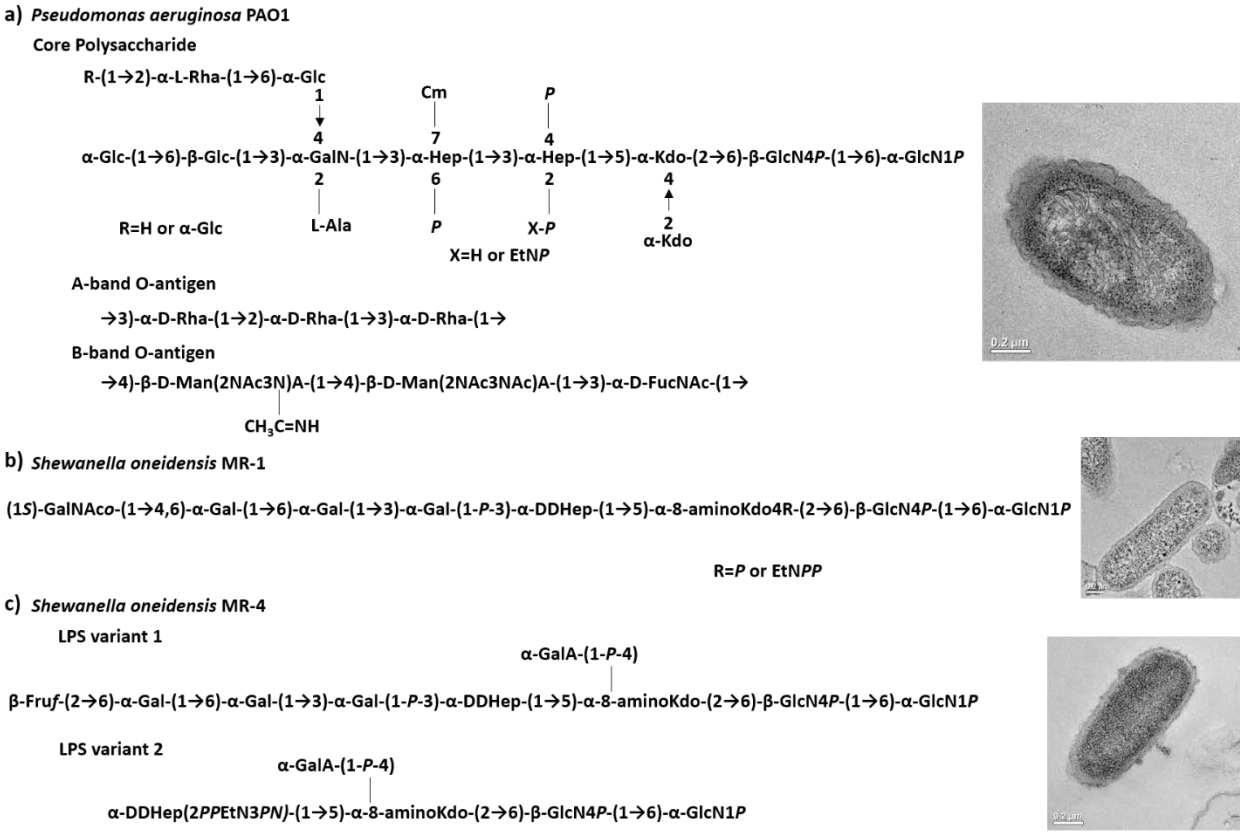

Figure S1. The structure of the polysaccharide portion of the LPS and a representative TEM image of a) *P. aeruginosa*.[6] This bacterium creates two different O-antigens, namely the A-band and B-band; the A-band has about 23 repeats and the B-band has over 50 repeats.[7] The saccharide region and representative TEM images of b) *S. oneidensis* MR-1[8] and c) *S. oneidensis* MR-4. *S. oneidensis* MR-4 expresses two variants for its core polysaccharide structure.[9] These structures have been adapted from references.[6–9] The structures of the polysaccharide portion of LPS for *A. vinelandii* and *A. baylyi* are not as well characterized and are therefore not shown here.

S2. Citrate-capped AuNP Synthesis

4-nm-diameter citrate-capped AuNPs were synthesized using a flow reactor based on modified procedures that have been previously reported.[1,2] Briefly, 20 mL of 0.01 M $HAuCl_4$ was added to

1600 mL nanopure deionized water in a 2 L Erlenmeyer flask to make the gold precursor solution. At the same time, 10 mL of 0.1 M $NaBH_4$ was added to 1616 mL of chilled nanopure deionized water in another 2 L Erlenmeyer flask. 6 mL of 0.1 M sodium citrate was added to the gold precursor solution prior to the synthesis. Both the gold precursor solution and sodium borohydride solution were put through a flow reactor (peristaltic pump) at 40 mL/min into a 4 L jug with gentle stirring. Once the two solutions were combined in the reactor lines, the resulting solution became a light pink color, and was stirred for at least 1 h before using. The diameters of citrate-capped AuNPs were determined in suspension by UV–vis extinction spectroscopy (Fig. S2) to be around 4 nm.[3]

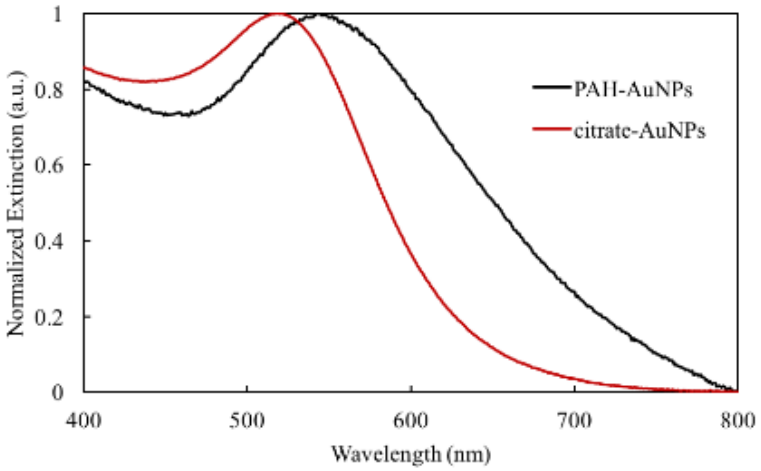

Figure S2. UV-vis extinction spectra for citrate-capped AuNPs and PAH AuNPs.

S3. Quantification of free PAH

To wrap the AuNPs with PAH, a suspension containing excess PAH was mixed with the citrate-capped AuNPs. Purification via centrifugation was performed on the resulting PAH AuNP suspension, however, some of the excess PAH remained in the suspension as well. Quantification of the leftover free PAH in the AuNP suspension was quantified so that relevant free PAH controls

could be completed in this study. The concentration of free PAH in the AuNP suspension was determined using a fluorescamine assay as described previously.[4] Briefly, the samples were first centrifuged at 66,000×*g* for 45 min at 4 °C to remove all of the AuNPs. The supernatant was removed and concentrated using a Savant Speedvac concentrator. Then, 120 µL of the sample was mixed with 20 µL of sodium borate buffer (pH 8) and 60 µL of 0.1% (w/v) fluorescamine in acetonitrile in a 96 well plate. The reaction occurred at room temperature for 5 min before the fluorescence was detected using a plate reader that excited at 425 nm and quantified the emission at 480 nm. The fluorescence detected was converted to a PAH concentration with the use of a calibration curve. With the use of the fluorescamine assay, the concentration of free PAH in the AuNP suspension was determined to be 7.53 ± 0.20 mg/L of PAH per mg Au/L of AuNPs. This information is critical for doing free PAH controls during toxicity experiments.

S4. Association of PAH AuNPs to bacterial surfaces

Bright field TEM was used to visualize the association of PAH AuNPs with the different bacterial surfaces. The use of dark field TEM imaging aided the identification of the AuNPs as their high crystallinity greatly improves their contrast in dark field mode,[5] making them appear as bright spots amidst the bacterial matrix. The dark field images are shown in Fig. S3 and the bright spots (AuNPs) can be seen at the cell surfaces for each of the bacteria.

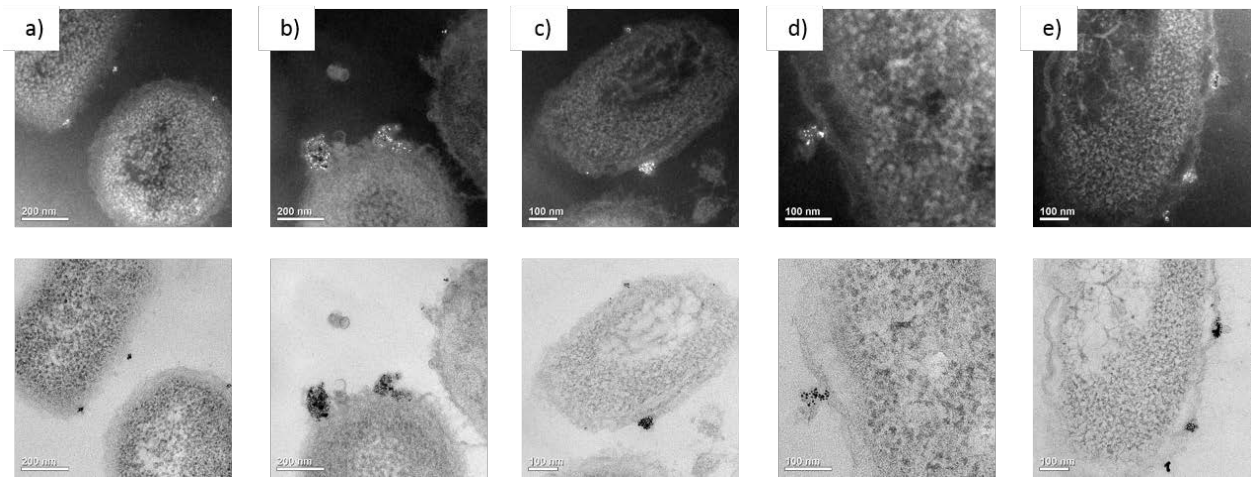

Figure S3. Dark field TEM images (top) highlighting the presence of PAH AuNPs (bright spots) due to their efficient scattering properties at particular diffraction angles, for a) *A. baylyi* ADP1, b) *A. vinelandii* UW, c) *P. aeruginosa* PAO1, d) *S. oneidensis* MR-1, and e) *S. oneidensis* MR-4. The bottom images are the corresponding bright field images.

S5. Flow Cytometry

To draw the gates to determine which bacterial population was bound by PAH AuNPs, a control sample of bacterial cells with SYTO9 stain that was not exposed to AuNPs was used. A representation of this data can be seen for *A. baylyi* in Fig. S4a. The bacterial cells are first distinguished from other debris by the presence of SYTO9 stain (top plot). The gate was then drawn using the scattering of the cells (bottom plot), as AuNPs have efficient scattering properties, which means cells bound to AuNPs have a higher forward and side scattering than bare bacterial cells. Therefore, the gate was drawn at the high edge of scattering for the bacterial cell controls for each species of bacteria. Using these gates, binding was seen for both *A. baylyi* and *A. vinelandii* at 0.0281 ppm PAH AuNP, demonstrating that binding can be observed at a lower dose of PAH AuNPs (Fig. S4b). At this PAH AuNP concentration, *A. vinelandii* shows higher AuNP binding than *A. baylyi*.

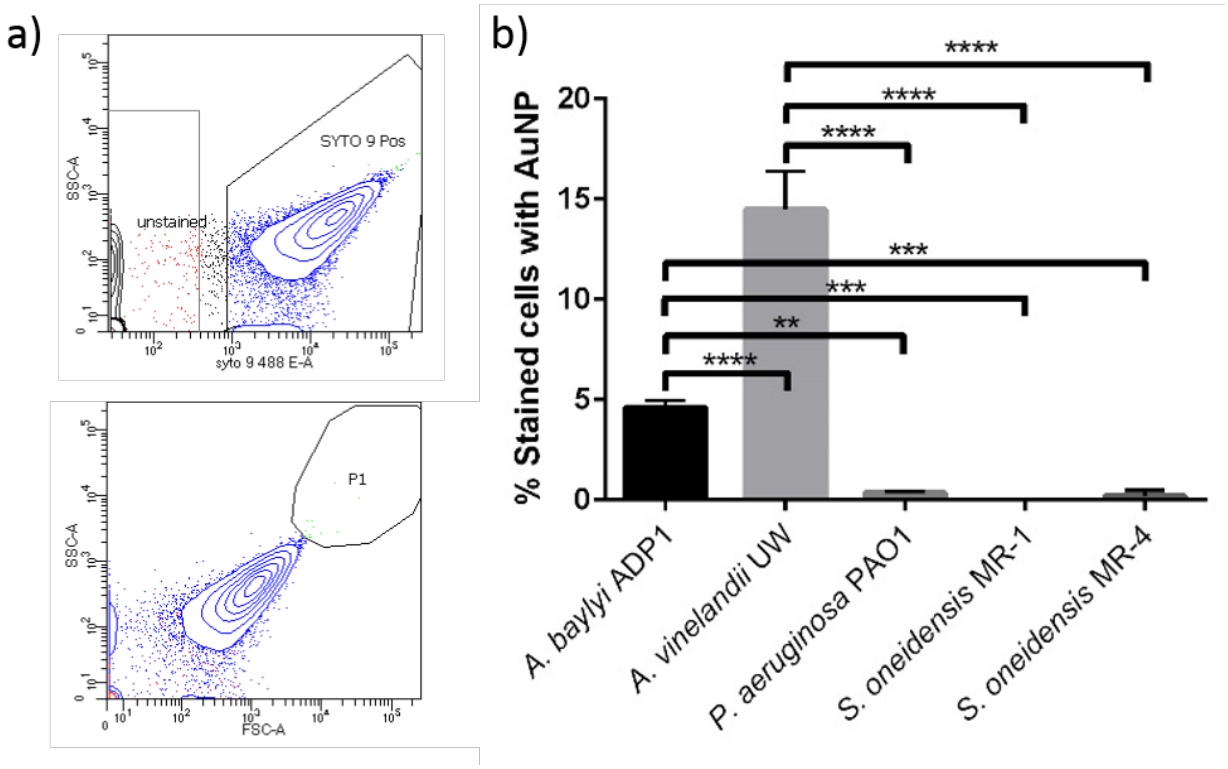

Fig. S4. Representative data for a) *A. baylyi* is shown to demonstrate how the gate determining PAH AuNP binding was drawn. With a sample of cells stained with SYTO9 and no AuNPs, the top plot was used to determine what events were bacterial cells based on the presence of SYTO9 stain. The bottom plot shows only events that had SYTO9 stain present, and the gate for AuNP binding was drawn at the high scattering edge of the events from this control experiment lacking AuNPs. This gate was used for all *A. baylyi* samples to determine PAH AuNP binding. From running flow cytometry, binding was also seen with some bacterial species even when exposed to b) a lower dose of PAH AuNPs (0.0281 ppm). **p<0.01, ***p<0.001, and ****p<0.0001.

S6. Distance between *P. aeruginosa* phosphorus atoms and the PAH center of mass

During the computational simulation of PAH association to the LPS constructs, the distance between phosphorus atoms in the *P. aeruginosa*, *E. coli*, and *S. typhimurium* LPS and the center of mass of the PAH molecule were monitored. The positions of these phosphorus atoms are shown in Fig. S5, and the graphs of these distances are shown in Fig. S6-S8. The PAH relaxes to equilibrium distances within the first 5 nanoseconds of the simulation. On average, P1 shows highest proximity to the PAH center of mass.

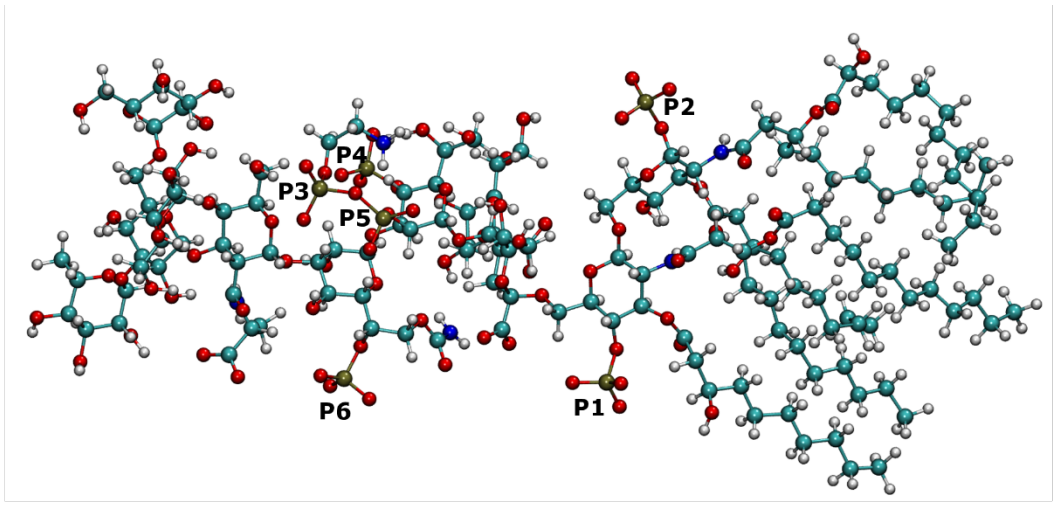

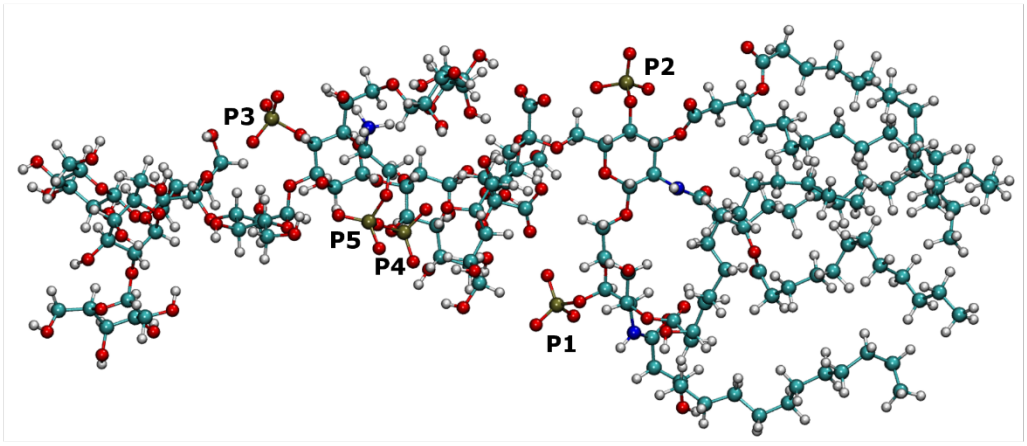

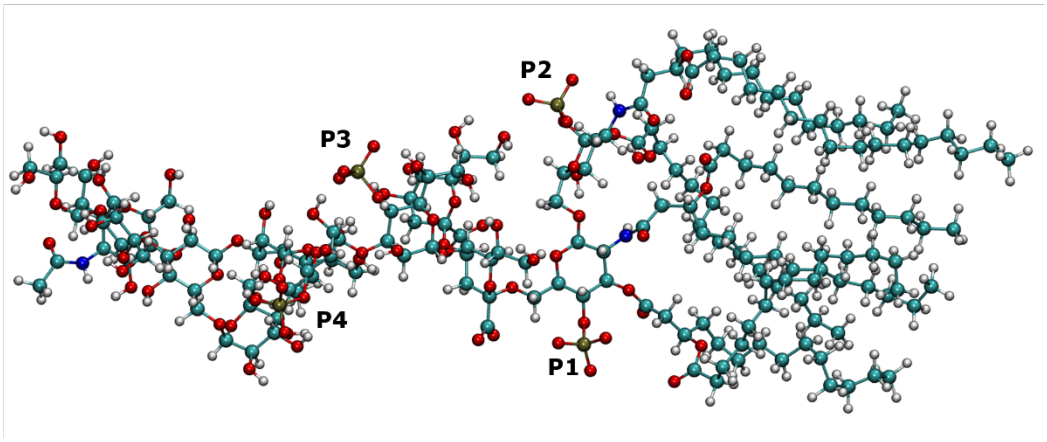

Figure S5. Ball-and-stick renderings of representative structures of rough LPS for a) *P. aeruginosa*, *E. coli*, and *S. typhimurium* with phosphorus atoms labeled as references for the numerical observables shown in Fig. S6-S8.

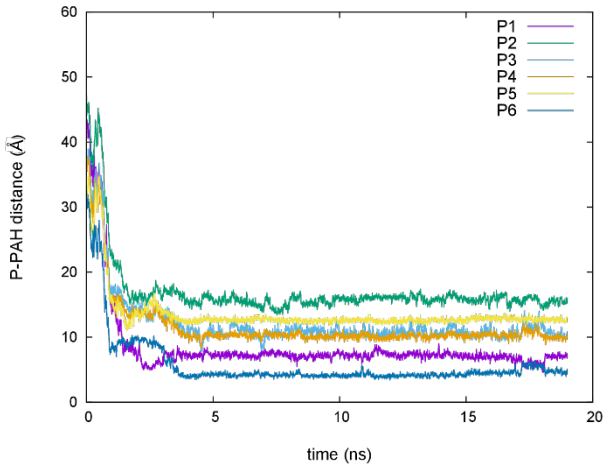

Figure S6. Distance between the PAH center of mass and 6 different phosphorus atoms labeled in panel a of Figure S5 in a rough *P. aeruginosa* LPS construct.

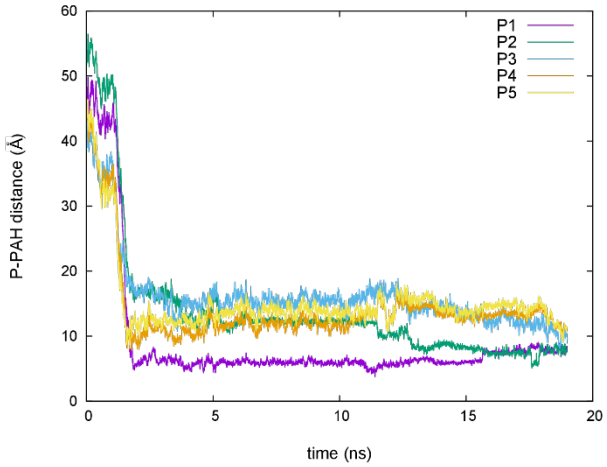

Figure S7. Distance between PAH center of mass and 5 different phosphorus atoms labeled in panel b of Figure S5 in a rough *E. coli* LPS construct.

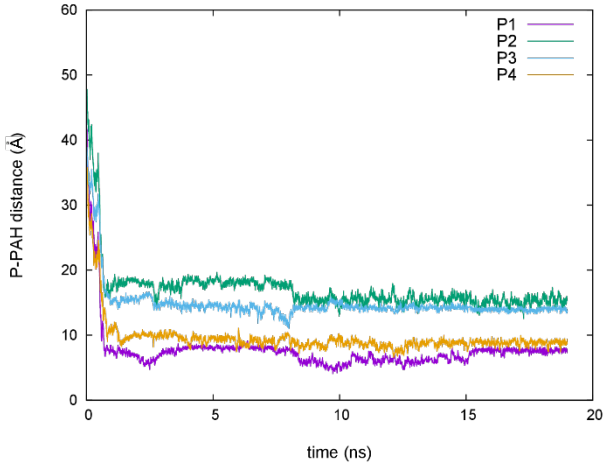

Figure S8. Distance between PAH center of mass and 4 different phosphorus atoms labeled in panel c of Figure S5 in a rough *S. typhimurium* LPS construct.

References

1 A. Gole and C. J. Murphy, *Chem. Mater.*, 2004, **16**, 3633–3640.

2 S. E. Lohse, J. R. Eller, S. T. Sivapalan, M. R. Plews and C. J. Murphy, *ACS Nano*, 2013, **7**, 4135–4150.

3 W. Haiss, N. T. K. Thanh, J. Aveyard and D. G. Fernig, *Anal. Chem.*, 2007, **79**, 4215–4221.

4 T. A. Qiu, M. D. Torelli, A. M. Vartanian, N. B. Rackstraw, J. T. Buchman, L. M. Jacob, C. J. Murphy, R. J. Hamers and C. L. Haynes, *Anal. Chem.*, 2017, **89**, 1823–1830.

5 N. D. Klein, K. R. Hurley, Z. V. Feng and C. L. Haynes, *Anal. Chem.*, 2015, **87**, 4356–4362.

6 G. B. Pier, *Int. J. Med. Microbiol.*, 2007, **297**, 277–295.

7 H. L. Rocchetta, L. L. Burrows and J. S. Lam, *Microbiol. Mol. Biol. Rev.*, 1999, **63**, 523–553.

8 E. Vinogradov, A. Korenevsky and T. J. Beveridge, *Carbohydr. Res.*, 2003, **338**, 1991–1997.

9 E. Vinogradov, J. Kubler-Kielb and A. Korenevsky, *Carbohydr. Res.*, 2008, **343**, 2701–2705.